# Adsorption and Decomposition Studies of *t*-Butylamine, Diethylamine, and Methylethylamine on Si(100)−(2 × 1)

**Jin-Bao Wu,[†] Yaw-wen Yang,*[,†,‡] Yi-Feng Lin,[†] and Hsin-Tien Chiu[†]**

*Department of Applied Chemistry, National Chiao-Tung University, Hsinchu, Taiwan 300, and National Synchrotron Radiation Research Center, Hsinchu, Taiwan 30077*

*Received: April 8, 2003; In Final Form: November 16, 2003*

We have studied chemisorption and thermal decomposition of *tert*-butylamine (TBA), diethylamine (DEA), and methylethylamine (MEA) on Si(100)−(2 × 1) with synchrotron-based X-ray photoelectron spectroscopy (XPS) and temperature programmed desorption (TPD). Adsorption at cryogenic temperature leads to molecularly intact chemisorption (dative-bonding via the nitrogen lone pair) and dissociative chemisorption via N−H scission, producing distinct N 1s peaks at binding energies of 401.1 and 398.2 eV, respectively. The corresponding change for C 1s core level is also significant, and a 0.9 eV shift toward lower binding energy is found for DEA, suggesting a high degree of charge redistribution between two adsorption configurations. Upon warming to room temperature, the adsorbed amines almost completely transform into dissociative chemisorbed forms. Thermal decomposition of TBA at elevated temperatures produces desorption species of isobutylene via $\gamma$-H elimination, hydrogen cyanide, and $H_2$. In comparison, DEA and MEA decompose thermally to desorb imine via $\beta$-H elimination, ethylene via $\gamma$-H elimination, hydrogen cyanide, and $H_2$. Eventually, silicon nitride and silicon carbide are formed. Distinct decomposition pathways lead to a C/N ratio variation among the products, with TBA yielding the lowest C/N ratio.

## Introduction

Reactions of organic molecules on semiconductor surfaces have received a great deal of attention recently due to their fundamental and technological importance.[1−4] Fundamentally, covalently bonded semiconductor surfaces tend to exhibit open structures and molecular bonding to these surfaces is rather localized and directional. In contrast, the atomic structures of metal surfaces tend to be closely packed and the molecular interaction to the metal surfaces can be delocalized. Therefore, it is important to understand the difference in surface chemistry between these two types of substrates. Technologically, organic functionalization of the semiconductor offers a means of modifying semiconductor surfaces yielding desirable surface properties, which may find applications in the areas of chemical sensors, surface pattering and molecular electronics.[2,4]

The stable reconstructed (2 × 1) structure of the Si(100) provides an interesting case in surface reaction chemistry.[5] For bulk-terminated Si(100), each surface atom would have two dangling bond orbitals. Upon reconstruction of the surface, the Si atoms in adjacent rows pair up to form the (2 × 1) arrays of dimers, leading to one dangling bond orbital per Si surface atom. The bonding between two dimer atoms can be described in terms of one strong $\sigma$ bond and one weak $\pi$ bond.[3,4] Moreover, the dimer bond axis tilts away from Si surface plane, resulting in a so-called asymmetrical dimer with significant charge transfer from the "down" dimer atom to the "up" dimer atom. This charge density inequality manifests itself in the differential reactivity of the dimer atoms toward unsaturated hydrocarbon adsorption.[3,4] The down dimer atom is electrophilic and acts as an electron acceptor in Lewis acid−base reactions, whereas the up dimer atom is nucleophilic and behaves like an electron donor in a Lewis reaction.

The chemical bonding of amines to Si(100)−(2× 1) is interesting owing to the presence of nitrogen lone-pair electrons. Through this nitrogen lone pair, amines can bond to the down atom of the Si dimer in a molecularly intact form. This bonding scheme gives rise to a highly electron-deficient environment around the nitrogen atom, similar to the case of quaternary ammonium salt. The N 1s core level for the amine assuming this so-called dative bonding to the Si surface is characterized by a rather high binding energy value of no less than 401 eV.[1,6,7] In competition with this dative bonding is the dissociative chemisorption of the amine. Previous theoretical and experimental studies indicate that, for short-chain amines, N−H bond scission is facile and occurs with virtually no barrier; in contrast, the N−C bond scission needs to surmount a significant barrier despite a larger exothermicity derived from N−C bond breaking.[4,6,8]

Chemical reactivity studies of organic amines adsorbed on semiconductor surfaces have been relatively scarce. Surface reactions of amines at high temperature often lead to the formation of important classes of materials, i.e., nitride and carbide. In the case of silicon nitride, its thin films have been used extensively in microelectronic industry as gate dielectrics, diffusion barriers, and insulators. Owing to the lack of systematic studies, questions related to their formation mechanism remain largely unanswered. For example, besides the aforementioned N−H and N−C bond breakings, there exist other bond scission processes, perhaps of no lesser importance, at elevated temperature and they include H-elimination and methyl elimination at different carbon sites. What is the relative importance among various bond-scission processes and how do these processes

* To whom correspondence should be addressed. Fax: +886-3-578-3813. Phone: +886-3-578 0281-7314. E-mail: yang@nsrrc.org.tw.
† National Chiao-Tung University.
‡ National Synchrotron Radiation Research Center.

10.1021/jp0349233 CCC: $27.50 
Published on Web 01/13/2004

lead to the differences in the final end products? How do these processes compare with those occurring on transition metal surfaces?

In this report, we present a detailed investigation of the chemisorption and thermal decomposition of organic amines on Si(100) through a combined study with temperature programmed desorption (TPD) and synchrotron-based X-ray photoelectron spectroscopy (XPS). These amines constitute the ligand part of our custom-synthesized metal nitride precursors that are used to grow nitride materials via chemical vapor deposition (CVD). The insight gained from the ligand surface chemistry is an essential ingredient needed to elucidate far more complicated surface chemistry undergone by the precursors.[9] The amines examined include a primary amine, *tert*-butylamine (TBA), and the secondary amines, diethylamine (DEA) and methylethylamine (MEA). Owing to the similarity in the structural and surface chemistry between MEA and DEA, the results for MEA will be presented in brevity, with the additional data included in the Supporting Information. In the end, plausible surface decomposition reaction mechanisms for the amines on Si(100) are proposed.

## Experimental Section

Experiments were performed in a mu-metal spherical chamber pumped by a 400 L/s turbomolecular pump and a 120 L/s ion pump with a chamber base pressure of better than $3 \times 10^{-10}$ Torr. Major instruments installed in the chamber included a differentially pumped quadrupole mass spectrometer (UTI 100 C), a low energy electron diffraction apparatus, a differentially pumped sputter ion gun, and a triple-channeltron electron energy analyzer (VG CLAM 2).

XPS measurements were carried out in the wide range spherical grating monochromator beamline (WR−SGM) of NSRRC. All of the reported XPS spectra were first normalized to the photon flux by dividing the recorded XPS signal with the photocurrent derived from a gold mesh situated in the beamline. The binding energy scale was referenced to the bulk Si $2p_{3/2}$ core level at a binding energy (b.e.) of 99.2 eV relative to Fermi level in order to facilitate comparisons with the published binding energies for the other elements. The photon energy was usually set to 580 eV unless noted otherwise. For measurements at cryogenic temperature, due to surface photovoltage effect, a rigid shift of Si 2p core level toward higher binding energy by ∼0.6 eV had to be corrected for the *n*-type sample used here.[10] In TPD, up to fifteen different ions could be simultaneously measured by means of multiplexed control in software and the ionization region was enclosed by a copper, liquid-nitrogen-cooled shroud to reduce the hydrocarbon background further.

Two different methods for mounting the Si(100) sample (*n*-type $\rho = 1-10\ \Omega$ cm) were used. For the XPS measurements, a thin Si strip ($0.5 \times 5 \times 15$ mm$^3$) was mounted with its edges sandwiched between small Si pieces and thus-constructed edge assemblies were clamped down by two U-shaped Ta clips that also served as current leads for resistive heating.[11] This way, a uniformity of heating across the sample was achieved. In TPD measurements, a linear temperature ramp can be difficult to achieve due to the precipitous drop in resistivity at ∼450 K when thermal excitation of carriers becomes pronounced. In our arrangement, a flat Ta sheet (0.025 mm thick) was sandwiched tightly between two Si samples, and together they were held by two Ta clips from the edges. Initial heating was achieved by first passing current through the Ta sheet. At higher temperatures, when the Si sample became more conductive than the Ta sheet, then direct heating of the Si sample became possible. The linearity of sample heating was quite satisfactory and sample working temperatures could be varied between 100 and 1400 K. Thermocouples readings in both setups were calibrated against an optical pyrometer and published $H_2$ desorption temperature data.[12]

A standard procedure was followed to clean silicon sample, that is, a thorough outgassing of the holder at 900 K during the bakeout followed by a final silicon oxide removal at ∼1300 K in UHV and a slow cooling (−2 K/s) back to ambient temperature. After the experiments, the carbon and nitrogen contaminants were removed by Ar sputtering and annealing at ∼1100 K. TBA, DEA, and MEA were purchased from Aldrich. Dry molecular sieves were added to the amine samples to remove any residual water moisture and several freeze−pump−thaw cycles were also performed. The purity of the admitted gas was verified by in situ mass spectrometric analysis. The dosing of amines was performed with a capillary doser having a flux enhancement factor estimated as 30.

Despite the improvement in TPD instrument, we also utilized a linear algebra technique to analyze TPD data to reach a definitive species identification. It is well-known that a parent ion can simultaneously produce a number of daughter ions of mostly lower mass with distinct fragmentation ratios. Thus, an observation of a given mass does not constitute a direct proof that this species exists as an independent entity. For example, a finding of 16 amu species does not necessarily mean that methane exists; in fact, it could be equally likely that 16 amu species is simply derived from other heavier hydrocarbons. In the latter case, the TPD spectrum for 16 amu can be mathematically expressed as a linear combination of weighted parent ion spectra. Each weighting coefficient is simply proportional to the product of the ion fragmentation ratio (daughter/parent) and the population of parent ions. The technique of recovering these coefficients through matrix manipulation is termed singular value decomposition or principal component analysis (PCA) in linear algebra[13] that has found wide applications in problems of analytical chemistry interest.[14] An additional advantage gained from this analysis is that the number of independent ions (nonrelated through mass fragmentation processes) existing among a set of observed ions can be readily estimated, which is very useful in narrowing down the number of possible desorption products. A commercial software with PCA capability was used here.[15,16]

## Results

***t*-Buytlamine.** Figure 1 shows a set of TPD spectra obtained after exposing Si(100) to TBA of various dosages. A careful searching of the possible mass fragments was undertaken beforehand to make sure no desorption products escaped our detection. Results from principal component analysis suggest that about four or five independent species exist among the observed fragments. Due to the absence of parent ion (73 amu), the most massive fragment of $m/z = 58$ is selected to represent TBA. Figure 1A shows that the desorption of TBA starts from a small peak at 630 K and, at increasing dosage, smaller features appear in the lower temperature side besides the main desorption peak. At the highest dosage, an intense peak appears at 170 K, attributed to the desorption of physisorbed TBA.

The desorption profiles of $m/z = 56$ species, Figure 1B, are different from those of the 58 amu and only a small fraction of the signal is derived from higher masses, as concluded from a small desorption peak found for the physisorption state at 170 K. The 56 amu species is attributed to isobutylene and its intense

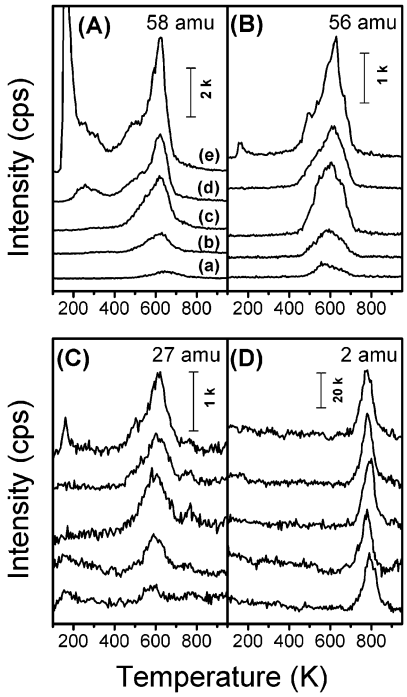


**Figure 1.** Coverage-dependent, multi-mass TPD spectra for the TBA dosed on Si(100). The TBA was dosed onto a 100 K surface with exposure for each curve as (a) 0.3 L, (b) 1.2 L, (c) 1.8 L, (d) 2.7 L, and (e) 3.6 L. The detected masses in the panels are (A) 58 amu, the largest observable mass fragment of TBA; (B) 56 amu, isobutylene; (C) 27 amu; and (D) 2 amu, $H_2$. Scale bar is shown to denote the relative magnitude of the ion intensity expressed in count per second (cps). To improve counting statistics for $H_2$ detection, the signal for low-mass end is purposely enhanced and cannot be directly compared with those for higher masses.

desorption feature spans a temperature region from 430 to 720 K, with the maximum desorption occurring at 610 K. For the desorption spectra of $m/z = 27$ species shown in Figure 1C, this species is mostly derived from those of isobutylene and TBA except for a small 760 K peak in which no contribution from higher masses can be found. This unique feature is attributed to hydrogen cyanide, HCN, evidenced by the presence of 26 amu species at the same temperature and with the same desorption profile.

Hydrogen atoms, generated from various C−H and N−H bond (see Figure 2) cleavages, eventually desorb as $H_2$, as shown in Figure 1D. Because $H_2$ desorption occurs at a higher temperature than the other fragments, it is not surprising to see that the $H_2$ desorption feature observed here closely resembles that found for $H_2$ desorption from clean Si(100)−(2 × 1). The single desorption peak at 780 K and the absence of the shoulder peak at 680 K, characteristic of dihydride desorption,[12] all suggest that H atoms adsorb in monohydride form, i.e., silicon dimers remaining intact during TBA adsorption. Additionally, a relatively constant $H_2$ desorption temperature independent of coverage, suggesting a first-order desorption kinetics, is also similar to monohydride desorption reported previously.[12,17] Owing to the presence of three $\gamma$-methyl groups in each TBA molecule, desorption products such as $HN{=}C(CH_3)_2$ (an imine, 57 amu), acetonitrile ($CH_3CN$, 41 amu), and methane formed from a sequence of $\gamma$-methyl elimination can be expected (nitrogen atom of the amine regarded as $\alpha$-position). However, no unambiguous evidence can be found for their existence.

Figure 2 shows the change of N 1s (A) and C 1s (B) XPS spectra with annealing temperature for a 3 L of TBA dosed

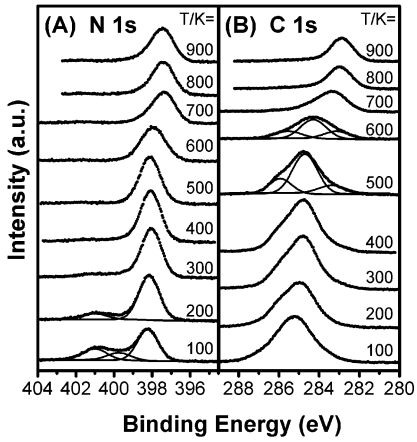


**Figure 2.** Variation of (A) N 1s and (B) C 1s XPS spectra with the annealing temperature for TBA chemisorbed on Si(100). Only selective fitting of C 1s spectra were carried out for the reasons stated in the text. The initial dosing of 3 L was done at 100 K.

onto Si(100). For the N 1s spectra presented in Figure 2A, the 100 K spectrum is composed of two distinct peaks and a third one in the valley. A warmup to 200 K causes the lower b.e. peak to grow in intensity at the expense of the other two higher b.e. peaks, as judged by peak area comparison. Similar intensity swapping among the peaks is also evident for the 300 K spectrum. Insight can be gained by the curve-fitting analysis that is based on nonlinear least squares algorithm. An integral Shirley background in conjunction with line shape functions generated from the products between Gaussian and Lorentzian functions are found to be adequate for describing the acquired spectra. In a given spectrum, the Gaussian with ($\Gamma_G$) and the Lorentzian width ($\Gamma_L$) are allowed to vary in the fits but are usually constrained to be the same for all peaks. The N 1s spectrum at 100 K can be decomposed into three components at 398.2, 399.7, and 401.1 eV. The peak at 399.7 eV is assigned to physisorption state due to its continuous intensity increase with the increasing dosage (data not shown). The other two main peaks located at 398.2 and 401.1 eV are interpreted as follows. Amine can bond to Si(100) in two distinct configurations: intact molecular adsorption via dative bonding and dissociative chemisorption via N−H bond breaking.[4,6,8] The former bonding is characterized by a high N 1s b.e. of 402.2 eV and the latter by a lower N 1s b.e. of 398.9 eV.[8] Therefore, it seems straightforward to assign our 398.2 eV peak to dissociatively chemisorbed TBA and the 401.1 eV peak to dative-bonded TBA, despite our b.e. values being consistently lower. It is not clear why this b.e. difference exists. At elevated temperatures, a marked change of both N 1s and C 1s spectra is to be expected owing to the formation of various desorption products. Surprisingly, relatively little change is noted for N 1s spectra other than a b.e. shift and a decrease of the peak intensity, perhaps caused by the small energy difference between N 1s peaks for chemisorbed TBA (398.2 eV) and surface $SiN_x$ (397.2 eV)[18,19] that is eventually formed. During the course of the annealing, the N 1s peak width decreases from 1.5 to 1.3 eV.

For C 1s XPS spectra, a complicated change of the peak features with annealing temperature is found. The C 1s peak for the chemisorbed TBA (300 K spectrum) is located at 284.9 eV, in agreement with reported value,[2] and has a peak width of 2.2 eV. After annealing to 500 K, the main peak not only broadens to 2.5 eV but also develops wings on both sides. Beyond 700 K annealing, the C 1s peak sharpens considerably and narrows down to 1.3 eV after 900 K annealing. An attempt of performing a detailed C 1s curve-fitting analysis aiming to

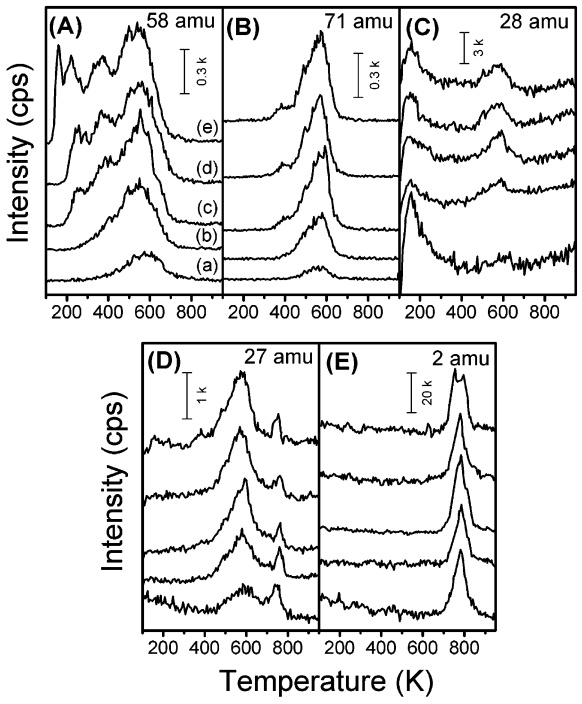


**Figure 3.** Multimass thermal desorption spectra for a Si(100)−(2× 1) preadsorbed with DEA of the varied dosage at 100 K: (a) 1.2 L, (b) 1.5 L, (c) 1.8 L, (d) 2.1 L, and (e) 3.6 L. The detected masses in the panels are (A) 58 amu, DEA; (B) 71 amu, *N*-ethyl-ethanimine; (C) 28 amu, ethylene; (D) 27 amu, predominately HCN; and (E) 2 amu, $H_2$.

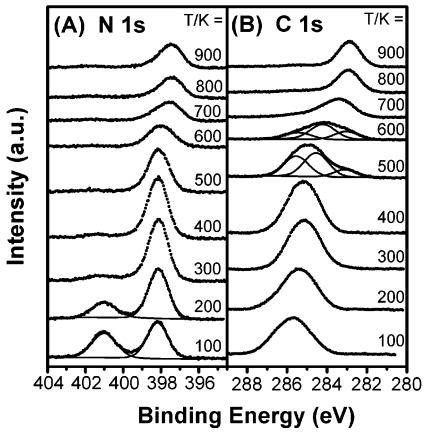


**Figure 4.** Change of (A) N 1s and (B) C 1s XPS spectra for the DEA dosed on Si(100) at 100 K for 3 L initially and later annealed to higher temperatures.

identify surface intermediates is met with great difficulty for the following reasons. For the amines used here, each amine molecule contains two distinct C 1s core levels owing to their different bonding environment. For instance, high-resolution C 1s spectrum acquired for chemisorbed diethylamine (310 K spectrum), presented in Figure 5B (vide infra), carries a distinct, nonsymmetrical signature, suggesting the presence of multiple peaks. Thus, a decomposition of this composite peak into two carbon components, one bonded to nitrogen and the other belonging to methyl group, is deemed satisfactory. With increasing complexity, even for high resolution spectrum such as the curve a of Figure 5B, a meaningful fitting still has to be carried out with great care based on a judicious choice of parameters. Unfortunately, carbon peaks are usually broadened by excitations from phonons, electronic shake-up and molecular vibration, poor instrumental resolution, etc. The resultant broad C 1s peak makes the curve fitting susceptible to large errors,

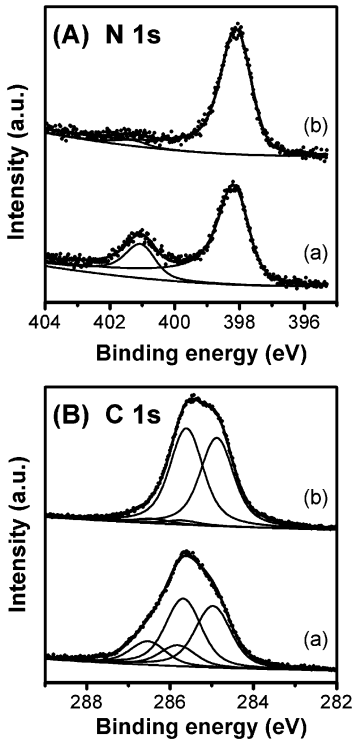


**Figure 5.** Curve fitting of N 1s (A) and C 1s (B) spectra to extract the binding energy difference between the DEA dissociatively chemisorbed on Si(100) and the DEA forming an adduct with down-atom of Si dimer. Curve a was taken at 180 K, whereas the curve b was at 310 K.

particularly when the number of species and their peak characteristics cannot be further constrained. In view of this severe limitation, we are refrained from delving too much into carbon peak fitting. Instead, a qualitative understanding is pursued by performing curve fitting only for those spectra with a distinct signature suggesting the presence of multiple components, such as 500 and 600 K spectra. The 600 K spectrum can be decomposed into three peaks at 285.6, 284.3, and 283.0 eV. The highest b.e. peak at 285.6 eV can be ascribed to a C−N group bonded to Si surface atom, the same as that obtained in Figure 5B. The 284.3 eV peak is associated with the alkyl group bonded to the Si surface.[2] The lowest b.e. peak at 283.0 eV is typically attributed to the carbidic species.[20] At the completion of the hydrocarbon desorption at a temperature higher than 700 K, the N 1s and C 1s peaks become much narrower and settle down to 397.5 and 282.9 eV, respectively. These b.e. values are characteristic of the silicon nitrides and silicon carbides; however, the possibility of forming silicon carbonitride cannot be ruled out.

**Diethylamine.** Figure 3 shows multimass TPD spectra for the Si(100)−(2× 1) dosed with DEA of different amounts at 100 K. A fragment of 58 amu is selected to represent the molecular desorption of DEA owing to its being the most abundant fragment. The desorption feature of 58 amu is the same as that of the parent DEA ion (73 amu). For a dosage of less than 1.2 L, a single desorption state with its peak-desorption temperature ($T_p$) at 550 K is observed. For the increasing dosage, a second desorption peak appears at 380 K. At a dosage larger than 1.8 L, a third desorption state appears at around 265 K. At the highest dosage of 3.6 L, a fourth desorption peak appears at 165 K, associated with the desorption of physisorbed DEA. Due to recombinative desorption nature, desorption kinetics for DEA could be second-order in principle. However, notable features derived from a second-order desorption process such

as the shift of $T_p$ toward lower temperature for the increasing dosage are missing. In fact, the desorption spectra exhibit a first-order like feature, particularly, the invariance of $T_p$ with respect to surface coverage. Employing the Redhead formalism[21] with the preexponential set at $10^{13}$, we derive at the following desorption energies for three desorption states (in the order of increasing $T_p$): 64, 101, and 153 kJ/mol, respectively.

In parallel with molecular desorption of DEA, different fragments are also produced and desorbed from the heated silicon surface. Figure 3B−E shows the thermal desorption of four distinct molecular fragments as a function of the dosage. Again, a careful, systematic searching of the possible decomposition products up to twice the mass number of the DEA turns up four distinct molecular fragments after consulting the cracking patterns of the fragments. The 71 amu species, presented in Figure 3B, is not a fragment of DEA and is attributed to *N*-ethyl-ethanimine ($C_2H_5N{=}CHCH_3$) that is formed via the $\beta$-H elimination of DEA. Note that the α site is counted from the N end of the amine. Major imine desorption appears at the same temperature range centered at 565 K, irrespective of surface coverage, but at higher surface coverage, a minor peak appears at near 400 K. The 28 amu signal (Figure 3C), partly derived from the fragment of DEA, still owes much of its presence to ethylene that is produced from the $\gamma$-H elimination of DEA adsorbate. The 27 amu signal (Figure 3D) is composed of two prominent features. A lower-temperature peak (<650 K) is completely derived from hydrocarbon fragments of higher masses, yet the distinct peak at 750 K is attributed to hydrogen cyanide (HCN). It is noted that, although HCN is formed through a sequence of bond breakings, it is quite a common decomposition product of many amines and nitrogen-containing compounds, both in gas-phase and surface-mediated decomposition reactions.[22−26] Finally, H atoms remaining on the silicon surface eventually desorb as $H_2$, as shown in Figure 3E. The $H_2$ desorption spectra again closely resemble those of monohydride on Si(100)−(2 × 1).

Figure 4 shows the changes of N 1s (A) and C 1s (B) XPS spectra with annealing temperature for a Si(100) dosed at 100 K with 1.5 L DEA. For the 100−300 K spectra, two N 1s peaks appear at the b.e. of 398.2 and 401.1 eV and they are again assigned to dissociatively chemisorbed DEA and dative-bonded DEA, respectively. Between 400 and 650 K, TPD data show that bond-breaking processes can lead to various decomposition products. This change of surface-bound species is reflected well in XPS data. As the annealing temperature is raised higher than 400 K, the intensity of N 1s peak at 398.2 eV starts to decrease and, at 600 K, drops to one-third of its value at 400 K. However, for the same temperature range, the b.e. shift of the peak is no more than 0.2 eV, suggesting that the bonding between Si and N remains intact. At annealing temperatures higher than 800 K, the N 1s peak settles down to a b.e. of 397.4 eV, close to the reported N 1s b.e. of 397.2 eV for $SiN_x$ films grown on Si substrate.[18,19] As for the Si 2p spectra, because of the high energy photons of 580 eV used here, the surface sensitivity is greatly reduced and the spectrum remains pretty much the same during the course of annealing.

Figure 4B shows the corresponding change of C 1s XPS spectra for DEA adsorbate. Based on the same reasoning as stated in the TBA subsection, only qualitative description instead of a detailed analysis of carbon spectra will be given here. At 100 K, C 1s peak is rather broad and has a width of 2.2 eV, with the peak centroid located at 285.7 eV. Warming up to 200 K shifts the C 1s peak toward lower b.e. by 0.3 eV but the similar peak characteristic is retained. A mild heating to 400 K shifts the peak centroid to 285.2 eV and this relatively small spectrum change agrees with the TPD result in which no desorption products can be found before reaching a surface temperature of 400 K. An annealing to 500 K reduces C 1s peak intensity and sees the emergence of a small peak at low b.e. of 283 eV. The 600 K annealing further reduces the peak intensity by 50% and shifts the peak centroid to 284.2 eV. The peak fitting confirms the presence of a carbide species at a binding energy of 282.8 eV, in line with reported C 1s b.e. values for silicon carbides that are quite varied: 282.5,[27] 283.4,[27] and 283.8 eV.[18,19] Further annealing shifts the peak toward lower b.e. with a concomitant narrowing of the peak. At 800 K, the C 1s peak already settles down to its final value of 282.8 eV with a width of 1.2 eV. A small peak having an intensity a few percent of that of the carbide peak is present at 285.5 eV. This small peak becomes discernible after the complete decomposition of DEA and is tentatively attributed to CN species. For the spectra taken between 500 and 700 K annealing, where significant spectral change occurs due to the existence of multiple species with peak characteristics largely unknown, it is difficult to reach an unequivocal species identification through peak decomposition. Nonetheless, it can be stated that a continuous lowering of C 1s b.e. with the annealing temperature suggests that the carbon atom continuously gains the electronic charge through developing a bonding to silicon atom of lowest electronegativity among three elements. The Pauling's electronegativity values are: 3.04 for N, 2.55 for C, and 1.90 for Si, respectively.

Previous density functional calculation[8] has indicated a high degree of ionic character in dative bonding formed between trimethylamine and Si(100)−(2 × 1). This change of electronic structure can manifest itself in terms of XPS b.e. shift. Previous study also showed that N 1s and C 1s core levels of both $CH_3$-CN and $C_2H_5NH_2$ when formed dative bonded adduct with $BF_3$ could shift toward higher b.e. by about 2 eV.[28] The present high-resolution XPS afforded by synchrotron-based XPS source offers an opportunity of examining this b.e. shift in greater details. Figure 5 shows a better-resolved N 1s (A) and C 1s (B) XPS spectra for the DEA undergoing interconversion from dative bonding at cryogenic temperature to dissociative chemisorption at ambient temperature. A dosing of 5.2 L DEA was carried out at 180 K to preclude the physisorption. The spectra were acquired at optimized photon energies of 320 eV for C 1s and 450 eV for N 1s. Figure 5A shows the presence of two N 1s peaks at 398.2 and 401.1 eV, with the latter having a 34% intensity of the former. Annealing to 310 K diminishes the latter peak to an intensity of 5% of the former, as shown in the curve b of Figure 5A.

Thanks to the better energy resolution, the corresponding C 1s spectra are also quite revealing; for instance, a temperature increase from 180 to 310 K reduces the intensity of the high b.e. shoulder considerably. In principle, two C 1s core levels exist in a given DEA molecule due to the varied electronic environment when an ethyl group is bonded to nitrogen atom and, additionally, there are two kinds of amines adsorbed on the surface. Thus, the C 1s spectra should be fitted with four peaks. The intensity ratio between two forms of the amine is fixed by consulting the corresponding N 1s peak ratio, i.e., 0.34 for 180 K and 0.05 for 310 K spectra. For each kind of amine, the intensity ratio of two carbon peaks should be close to 1:1, reflecting the carbon stoichiometry of the DEA molecule. A more elaborate curve fitting method is adopted here to extract peak parameters reliably. A nonlinear least-squares fitting is performed using a polynomial background in conjunction with a line shape function generated by a convolution of the Gaussian

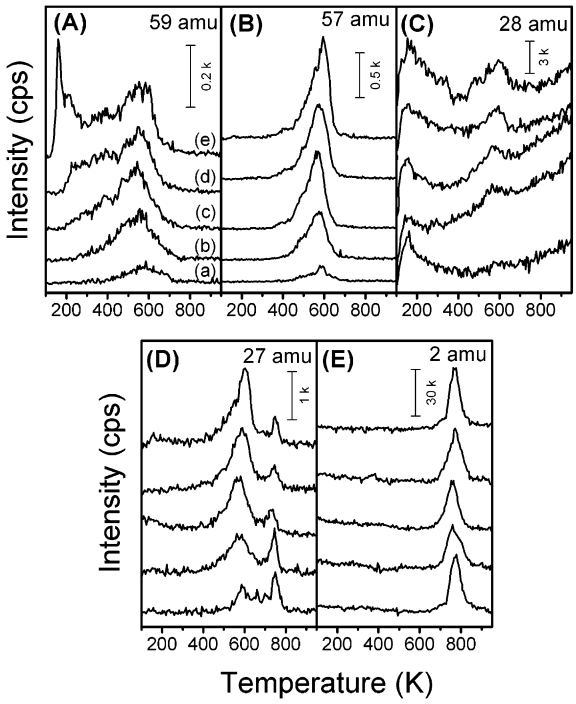


**Figure 6.** Coverage-dependent, multi-mass TPD spectra for the Si(100) predosed with varied amount of MEA at 100 K. The detected masses in the panels are (A) 59 amu, MEA (B) 57 amu, imine; (C) 28 amu; (D) 27 amu; and (E) 2 amu. The dosages for each curve are (a) 0.3 L, (b) 1.2 L, (c) 1.8 L, (d) 2.7 L, and (e) 3.6 L.

function with the Doniach−Sunjic (D−S) function broadened by a finite lifetime. Physically sound D−S function provides a better description of the photoemission background originated from inelastic loss processes in the solid than integral background of Shirley type does.[29] The fitting parameters, including a polynomial background, Gaussian width ($\Gamma_G$), Lorentzian width ($\Gamma_L$), and D−S asymmetric parameter ($\alpha$), are allowed to vary in the fits but are constrained to be the same for all the peaks. The derived parameters are $\Gamma_G = 0.76$ eV, $\Gamma_L = 0.40$ eV, and $\alpha = 0.02$. The b.e. difference between two carbon atoms in a given amine is determined to be 0.7 eV. For dissociatively chemisorbed amine, two C 1s peaks are located at 284.9 and 285.6 eV, respectively, with the one at low b.e. assigned to terminal methyl group and the other at higher b.e. attributed to the carbon in proximity to the nitrogen. For the dative-bonded amine, two C 1s levels are found at 285.8 and 286.5 eV, respectively, and they are shifted toward higher b.e. by 0.9 eV than those of the corresponding dissociatively chemisorbed amine. The fitted components and their sum together with the raw spectrum are displayed in the Figure 5.

**Methylethylamine.** Figure 6 shows a set of multi-mass TPD curves obtained from MEA adsorption on Si(100). MEA desorbs over a wide temperature range and behaves in a way similar to DEA, as shown in Figure 6A. The desorption envelop of MEA starts with a broad peak at 550 K at low dosage, continuously extends toward lower temperature at higher coverage, and eventually joints with the desorption peak from the physisorption state at 160 K. The peak desorption temperature for the pronounced feature at 550 K is relatively unaffected by the coverage change. In comparison, the 57 amu species derived from a single $\beta$-H elimination process desorbs in a narrower temperature starting from 400 to 650 K with a peak temperature at 585 K, as shown in Figure 6B. The contribution to the 57 amu fragment by the MEA parent ion is estimated to be less than 10% of parent ion; as a result, the observed 57 amu signal is dominated by imine itself. The imine can be *N*-ethylmethanimine ($C_2H_5N{=}CH_2$) and/or *N*-methyl-ethanimine ($CH_3CH{=}NCH_3$). However, the latter species is believed to be more stable owing to C=N bond location being closer to the middle of aliphatic chain. The next lighter desorption product stemmed from C−C bond scission is acetonitrile, $CH_3CN$. However, we cannot reach a positive identification of this species through the PCA analysis. Figure 6C shows the desorption of ethylene that is produced from $\gamma$-H elimination in the ethyl group. Part of the 28 amu signal comes from the cracking fragments of higher masses and the contribution by ethylene cannot be certain. However, the one-third portion of the peak lying in the high temperature side can be judged as from ethylene. The desorption of hydrogen cyanide, HCN (27 amu), is presented in Figure 6D. The main constituent of the spectra is again deemed to be from cracking fragments of 59 and 57 amu species; however, the highest-temperature peak at 740 K is unique on its own and entirely attributed to HCN. The identity of HCN is evidenced by the same desorption profile for 26 amu. Finally, hydrogen molecules desorb from monohydride phase with its peak desorption temperature at 780 K.

Change of N 1s (A) and C 1s (B) XPS spectra with annealing temperature for the MEA is presented as Figure 1S in the Supporting Information owing to the similarity MEA bears with the DEA. In brief, only a heating to a temperature higher than 500 K does one start to observe significant changes in N 1s and C 1s spectra: intensity reduction accompanied by the peak broadening and the gradual shift of the peaks toward lower b.e value. At a temperature higher than 800 K, the carbide peak at the C 1s b.e. of 282. 8 eV and nitride peak at the N 1s peak of 397.4 eV develop to a near completion. These XPS spectra change is in accord with the change expected based on TPD data.

## Discussion

The amines reported in the present study belong to the class of either primary amine (TBA) or secondary amine (DEA and MEA), depending on the number of alkyl groups bonded to nitrogen. Because one motive for the present study is closely linked to enhancing our understanding of the surface reaction of metal nitride CVD precursors, we limit our studies to primary and secondary amines due to their exclusive use as ligands in synthesizing metal nitride precursors.[9] Previous studies undertaken with XPS, IR, and density functional calculations[4,6,8] establish a preferential N−H bond cleavage over N−C bond cleavage for the primary and secondary amines when dissociatively chemisorbed on Si(100), resulting in a characteristic N 1s peak at 398.9 eV.[8] For a tertiary amine such as trimethylamine reported earlier,[8] owing to the lack of H atom directly bonded to N atom, the dative bonded adduct persists to higher temperature of 600 K while the concomitant decomposition of the amine takes place.

In relation to the adsorption configuration for amines on Si(100)−(2 × 1), our high resolution XPS data have several interesting implications. For dissociatively chemisorbed amine, the N 1s peaks are found to locate at the same b.e. of 398.2 eV with almost the same width of 1.2 eV for all three amines at temperatures ranging from 100 to 300 K. The identical peak characteristics indicate that the same local electronic structure around N atoms exists despite a variation of the neighboring alkyl groups in those amines. Moreover, Figure 5 shows that both N 1s and C 1s core levels shift toward lower b.e by 2.9 and 0.9 eV, respectively, as the dative bonded DEA is transformed into dissociatively chemisorbed DEA. Density

functional calculation of trimethylamine (TMA) adsorption on Si(100)−(2 × 1)[8] shows that the valence charge distribution is greatly perturbed as the dative bonded TMA is formed. The charge transfer starts from the amine via the down atom to the up atom of the same silicon dimer, essentially piling up lone pair charge at the up atom of the dimer, thereby imparting electron acceptor property to the dimerized silicon surface. Charge depletion at the nitrogen atom is the greatest, resulting in a high b.e. shift of 2.9 eV. A shift of 0.9 eV for C 1s is also quite significant. The large shifts for N 1s and C 1s indicate that the charge redistribution is not restricted to nitrogen atom alone and is rather extensive as DEA bonding to Si(100) is altered.

The observation of a single N 1s peak at 398.2 eV provides an additional proof that bond scission occurs at N−H, not N−C bond as the amines, specifically TBA, is dissociatively chemisorbed on Si(100). If N−C bond breaking in TBA were to proceed, then the surface-bound species would be $C(CH_3)_3$(a) and $NH_2$(a). The N 1s b.e. for $NH_2$(a) on Si(100) is 397.4 eV and is lowered by 2 eV in comparison with that of $NH_3$(a) on Si(100).[30] Our observation of a consistent single peak at 398.2 eV clearly shows this N−C bond breaking does not occur. As N−H bond scission occurs exclusively, the detached H atom is most likely bonded to an adjacent Si atom belonging to the same dimer. The argument for the Si dimer being preserved is supported by the observation of monohydride desorption at high temperature, which indicates that dimer bond is not broken in the present adsorption experiment. The preservation of dimer bonding in molecular chemisorption seems to be a common occurrence and the reported cases include methyl iodide,[31] silanes,[32,33] phosphine,[34] etc.

Chemisorbed amines can decompose via several characteristic pathways at higher surface temperature. In the case of TBA, the $\gamma$-H elimination leads to isobutylene and a nitrided surface. If the $\gamma$-H elimination is the sole reaction path, the silicon surface can be expected to be free of carbon residue. In a previous study of *tert*-butylphosphine adsorption on Si(100), isobutylene and hydrogen desorption were found, yet no carbon could be detected after experiment, indicating the efficacy of $\gamma$-H elimination in removing carbons.[34] The present XPS data show the persistence of carbon, implying that other minor reaction pathways must be in place to account for the carbon presence. Earlier studies have shown that methyl[31,35] and ethyl adsorbates[33] cannot be directly desorbed from a Si(100); instead these adsorbates further dehydrogenate at high temperatures, liberating molecular hydrogen and producing Si−C surface species. Taking this into consideration, we believe that the minor reaction pathways could involve C−C scission, which eventually produces small hydrocarbon species and makes difficult their removal from the silicon surface afterward. The surface decomposition of TBA is summarized in Scheme 1.

For the cases of DEA and MEA, their decomposition pathways are expected to be similar due to their structural resemblance. The $\beta$-H elimination, prevalent in straight chain hydrocarbons on metal surfaces[36,37] but not possible in TBA due to a lack of hydrogen at the $\beta$-site, becomes a viable route for DEA and MEA. As-derived products are *N*-ethyl-ethanimine and *N*-methyl-ethanimine, accordingly. Meanwhile, the H-elimination at different places such as the $\gamma$ site can lead to ethylene formation in both DEA and MEA cases, as observed in Figures 3C and 6C. Smaller adsorption species such as Si−$NC_2H_5$ and Si−$NCH_3$ can be produced after removing the ethyl group from DEA and MEA, respectively. Through a series of dehydrogenation reactions, the formation of $CH_3CN$ and HCN

**SCHEME 1: Proposed Thermal Decomposition and Desorption Routes for TBA Adsorbed on Si(100).**

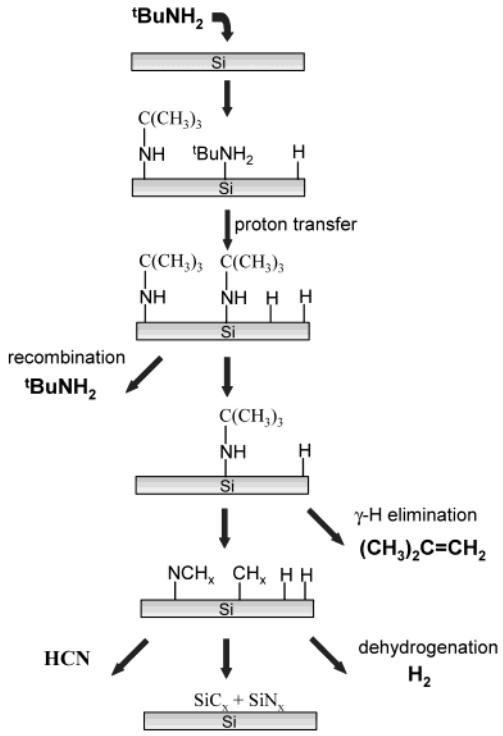


can be accomplished on the surface. While compelling evidence, particularly at 750 K, is found for HCN desorption, no conclusive proof can be found for acetonitrile desorption. The desorption profile of acetonitrile seems to be no more than a linear superposition of desorption spectra of parent amine and imine. The reason for the missing acetonitrile desorption is not clear. Finally, throughout the experiment, no $CH_4$ desorption can be observed for two amines, in agreement with an earlier report.[31] Scheme 2 summarizes the decomposition of DEA on Si(100) and the corresponding reactions for MEA are similar and hence omitted here.

It will be of interest to compare the amounts of carbon and nitrogen left on the silicon surface after the amines completely decompose at 900 K. Table 1 presents the fractions of carbon and nitrogen atoms remained by normalizing with respect to their initial values at 300 K to eliminate the possible coverage variation. The carbon-to-nitrogen ratio for the residue, $C_{900}/N_{900}$, is calculated by recognizing $C_{300}/N_{300}$ as the stoichiometric C/N ratio of intact amine. MEA gives rise to a product containing the least amount of carbon and nitrogen; whereas TBA leads to a product richest in carbon and nitrogen. However, TBA generates a product of the smallest C/N ratio. TBA and DEA can be further compared because they both have the same initial C/N ratio of 4:1. The decomposition product derived from TBA contains significantly more nitrogen, but same carbon contents, as compared with those of DEA. This trend can be rationalized as follows. The only viable elimination pathway for TBA is the $\gamma$-H elimination that removes four carbon atoms but leaves the nitrogen atom intact. In contrast, $\beta$-H elimination in both DEA and MEA can remove carbon and nitrogen at a ratio same as those of their molecular forms. Therefore, it is not surprising to observe that the TBA product has the highest nitrogen content and lowest C/N ratio. The retention of nitrogen atom is a unique attribute of TBA decomposition.

In comparing DEA and MEA of similar structures, MEA clearly gives rise to lower carbon and nitrogen contents and smaller C/N ratio. Besides prevalent $\beta$-H elimination, the other

**SCHEME 2: Proposed Thermal Decomposition and Desorption Routes for DEA Adsorbed on Si(100).**

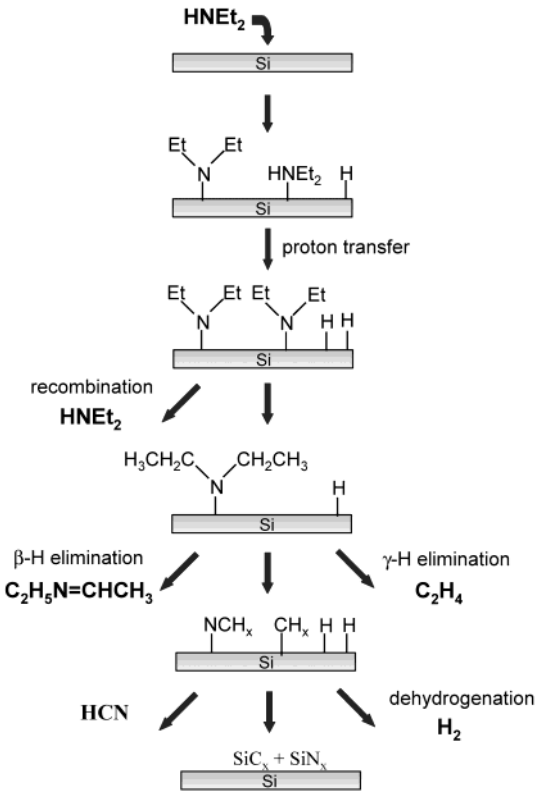


**TABLE 1: Carbon Fraction ($C_{900}/C_{300}$), Nitrogen Fraction ($N_{900}/N_{300}$), and Carbon to Nitrogen Ratio ($C_{900}/N_{900}$) after the Decomposition Completed at 900 K[a]**

| | TBA | DEA | MEA |
|---|---|---|---|
| $C_{900}/C_{300}$ | 0.30 | 0.32 | 0.18 |
| $N_{900}/N_{300}$ | 0.71 | 0.40 | 0.24 |
| $C_{900}/N_{900}$ | 1.69 (4) | 3.20 (4) | 2.25 (3) |

[a] Data compiled from XPS results shown in Figures 2, 4, and 1S. The numbers in parentheses are stoichiometric ratios of C/N for intact amines and are equal to $C_{300}/N_{300}$.

notable H elimination at the $\gamma$ site leading to the ethylene is also possible for both. However, MEA enjoys a particular advantage here because its fragment, after ethylene removal, is $-NCH_3$, that seems to be a more direct precursor to HCN, as compared with $-NC_2H_5$ derived from DEA. This small structural difference perhaps results in the product difference found between DEA and MEA. Finally, the present results can be utilized in optimizing the molecular design of metal nitride CVD precursors in which a transition metal center is joined by amido ($-$NR, R alkyl group) and/or imido ($=$NR) group to form volatile metal complexes. Based on the present results, the *tert*-butyl group or the methyl group is clearly a better choice over diethyl to effect a lower carbon content in metal nitride films, a clear benefit in reducing the interconnect resistance in electronic circuits.

In summary, the adsorption of TBA, DEA, and MEA on Si(100)$-(2\times 1)$ is predominately dissociative at room temperature via N$-$H bond cleavage. The amines can also be chemisorbed in a molecularly intact form, particularly at cryogenic temperature, and this adsorption is characterized by the dative-bonding to down atom of silicon dimer, as proposed earlier.[4,6,8] The two different types of chemical bonding are characterized by distinct N 1s core level binding energy, with the former at 398.2 and the latter at 401.1 eV. At elevated temperatures, recombinative desorption and molecular decomposition of all three amines take place, producing distinct desorption products. Principal component analysis was employed to help verify the independent existence of various products. TBA decomposes predominately via the $\gamma$-hydride elimination to generate isobutylene, hydrogen cyanide, and $H_2$. In comparison, DEA and MEA are found to decompose to produce imine (via $\beta$-H elimination), ethylene (via $\gamma$-H elimination), hydrogen cyanide (dehydrogenation), and $H_2$. Heating to 900 K results in silicon nitrides and silicon carbides on the surface. The H-elimination pathways prevalent in amine adsorption on Si(100) cases are similar to what are commonly observed for hydrocarbon adsorption on metal surfaces. Due to the efficient removal of carbon species by $\gamma$-H elimination, TBA gives rise to a lowest carbon-to-nitrogen ratio among all three amines.

**Acknowledgment.** We thank beamline group at SRRC for arranging to make the initial experiments possible during the commissioning of the wide-range beamline. Special thanks are due to S. C. Chung for developing TPD software. Both YWY and H.T.C. acknowledge the support by the National Science Council of R. O. C. through Grants NSC89-2113-M-213-015 and NSC-90-2113-M-009-022, respectively.

**Supporting Information Available:** Figure 1S shows the dependence of (A) N 1s and (B) C 1s XPS spectra with the annealing temperature for MEA chemisorbed on Si(100). This material is available free of charge via the Internet at http://pubs.acs.org.

## References and Notes

(1) Liu, H.; Hamers, R. J. *Surf. Sci.* **1998**, *416*, 354.
(2) Bergerson, W. F.; Mulder, J. A.; Hsung, R. P.; Zhu, X. Y. *J. Am. Chem. Soc.* **1999**, *121*, 454.
(3) Cao, X.; Coulter, S., L.; Ellison, M. D.; Liu, H.; Liu, J.; Hamers, R. J. *J. Phys. Chem. B* **2001**, *105*, 3759.
(4) Bent, S. F. *J. Phys. Chem. B* **2002**, *106*, 2830.
(5) Waltenburg, H. N.; Yates, J. T., Jr. *Chem. Rev.* **1995**, *95*, 1589.
(6) Mui, C.; Wang, G. T.; Bent, S. F.; Musgrave, C. B. *J. Chem. Phys.* **2001**, *114*, 10170.
(7) Cao, X.; Hamers, R. J. *J. Phys. Chem. B* **2002**, *106*, 1840.
(8) Cao, X.; Hamers, R. J. *J. Am. Chem. Soc.* **2001**, *123*, 10988.
(9) Wu, J.-B.; Yang, Y.-W.; Lin, Y.-F.; Chiu, H.-T. *J. Vac. Sci. Technol. A* **2003**, *21*, 1620.
(10) Landemark, E.; Karlsson, C. J.; Chao, Y. C.; Uhrberg, R. I. G. *Phys. Rev. Lett.* **1992**, *69*, 1588.
(11) Nishino, H.; Yang, W.; Dohnálek, Z.; Ukranitsev, V. A.; Choyke, W. J.; Yates, J. T., Jr. *J. Vac. Sci. Technol. A* **1997**, *15*, 182.
(12) Sinniah, K.; Sherman, M. G.; Lewis, L. B.; Weinberg, W. H.; Yates, J. T., Jr.; Janda, K. C. *J. Chem. Phys.* **1990**, *92*, 5700.
(13) Press, W. H.; Flannery, B. P.; Teukolsky, S. A.; Vetterling, W. T. *Numerical Recipes, The Art of Scientific Computing*; Cambridge University Press: Cambridge, U.K., 1986.
(14) Malinowski, E. R. *Factor Analysis in Chemistry*, 2nd ed.; Wiley & Sons: New York, 1991.
(15) Ressler, T. *WinXAS*; version 2.3., 2002.
(16) Ressler, T.; Wong, J.; Roos, J.; Smith, I. L. *Environ. Sci. Technol.* **2000**, *34*, 950.
(17) Gates, S. M.; Kunz, R. R.; Greenlief, C. M. *Surf. Sci.* **1989**, *207*, 364.
(18) Ermolieff, A.; Bernard, P.; Marton, S.; da Costa, J. C. *J. Appl. Phys.* **1986**, *60*, 3162.
(19) Ishidzuka, S.; Igari, Y.; Takaoka, T.; Kusunoki, I. *Appl. Surf. Sci.* **1998**, *130−132*, 107.
(20) Moulder, J. F.; Stickle, W. F.; Sobol, P. E.; Bomben, K. D. In *Handbook of X-ray Photoelectron Spectroscopy*; Chastain, J., Ed.; Perkin-Elmer Corp.: Eden Prairie, MN, 1992.
(21) Redhead, P. A. *Vacuum* **1962**, *12*, 203.
(22) Loh, K.; Jackman, R. B.; Loh, K. P.; Foord, J. S.; Kingsley, C. R. *Surf. Sci.* **1995**, *341*, 92.
(23) Somers, J. S.; Bridge, M. E. *Surf. Sci.* **1985**, *159*, L439.
(24) Hamada, Y.; Takeo, H. *Appl. Spectrosc. Rev.* **1992**, *27*, 289.

(25) Chen, J. J.; Winograd, N. *Surf. Sci.* **1995**, *326*, 285.
(26) Gardin, D. E.; Somorjai, G. A. *J. Phys. Chem.* **1992**, *96*, 9424.
(27) Smith, K. L.; Black, K. M. *J. Vac. Sci. Technol. A* **1984**, *2*, 744.
(28) Barber, M.; Connor, J. A.; Guest, M. F.; Hillier, I. H.; Schwarz, M.; Stacey, M. *J. Chem. Soc., Faraday Trans. 2* **1973**, *69*, 551.
(29) *Practical Surface Analysis: Vol. 1-Auger and X-ray Photoelectron Spectroscopy*; 2nd ed.; Briggs, D., Seah, M. P., Eds.; Wiley & Sons: Chichester, U.K., 1994.
(30) Dufour, G.; Rochet, F.; Roulet, H.; Sirotti, F. *Surf. Sci.* **1994**, *304*, 33.
(31) Gutleben, H.; Lucas, S. R.; Cheng, C. C.; Choyke, W. J.; Yates, J. T., Jr. *Surf. Sci.* **1991**, *257*, 146.
(32) Darlington, W.; Foster, M.; Campion, A. *Surf. Sci.* **1994**, *304*, L407.
(33) Schmidt, J.; Stuhlmann, C.; Ibach, H. *Surf. Sci.* **1994**, *302*, 10.
(34) Kaneda, G.; Murata, J.; Takeuchi, T.; Suzuki, Y.; Sanada, N.; Fukuda, Y. *Appl. Surf. Sci.* **1997**, *113/114*, 546.
(35) Kong, M. J.; Lee, S. S.; Lyubovitsky, J.; Bent, B. E. *Chem. Phys. Lett.* **1996**, *263*, 1.
(36) Zaera, F. *Chem. Rev.* **1995**, *95*, 2651.
(37) Bent, B. E. *Chem. Rev.* **1996**, *96*, 1361.